Cell, Vol. 113, 609–620, May 30, 2003, Copyright ©2003 by Cell Press

Mechanism of Ubiquitin Recognition by the CUE Domain of Vps9p

Gali Prag,[1] Saurav Misra,[1,4] Eudora A. Jones,[1,3] Rodolfo Ghirlando,[1,3] Brian A. Davies,[2,3] Bruce F. Horazdovsky,[2] and James H. Hurley[1,*]
[1]Laboratory of Molecular Biology
National Institute of Diabetes and Digestive and Kidney Diseases
National Institutes of Health
Department of Health and Human Services
Bethesda, Maryland 20892
[2]Department of Biochemistry and Molecular Biology and
The Mayo Clinic Cancer Center
Mayo Foundation
200 First Street SW
Rochester, Minnesota 55905

Summary

Coupling of *u*biquitin conjugation to *E*R degradation (CUE) domains are ~50 amino acid monoubiquitin binding motifs found in proteins of trafficking and ubiquitination pathways. The 2.3 Å structure of the Vps9p-CUE domain is a dimeric domain-swapped variant of the ubiquitin binding UBA domain. The 1.7 Å structure of the CUE:ubiquitin complex shows that one CUE dimer binds one ubiquitin molecule. The bound CUE dimer is kinked relative to the unbound CUE dimer and wraps around ubiquitin. The CUE monomer contains two ubiquitin binding surfaces on opposite faces of the molecule that cannot bind simultaneously to a single ubiquitin molecule. Dimerization of the CUE domain allows both surfaces to contact a single ubiquitin molecule, providing a mechanism for high-affinity binding to monoubiquitin.

Introduction

The covalent addition of ubiquitin and ubiquitin-like proteins is one of the most widespread regulatory post-translational modifications of proteins (Hershko and Ciechanover, 1998; Hochstrasser, 2000; Pickart, 2001). Ubiquitin is a 76 amino acid protein named for its extraordinary distribution from yeast to man. The C terminus of ubiquitin is conjugated to Lys residues of target proteins by the action of three enzymes: an ubiquitin-activating enzyme (E1), an ubiquitin-conjugating enzyme (E2), and an ubiquitin protein ligase (E3).

Ubiquitin is conjugated to proteins via an isopeptide bond between the C terminus of ubiquitin and a specific Lys residue in the ubiquitinated protein. Ubiquitin may be attached to proteins as a monomer or as a polyubiquitin chain. Ubiquitin polymers are formed when additional ubiquitin molecules are attached to Lys residues on a previously attached ubiquitin, usually Lys-48. Historically, interest in ubiquitination has centered on the role of polyubiquitin chains in targeting proteins for degradation by the 26S proteasome. It is now clear that ubiquitination regulates a much wider array of cell processes, including cell-cycle control, stress response, DNA repair, signaling, transcription, and gene silencing. Recently, intense interest has centered on the role of monoubiquitination as a sorting signal and regulator of endocytosis and endocytic trafficking, spurred in part by the discovery of new monoubiquitin recognition motifs (Shih et al., 2000; Katzmann et al., 2001; Hicke, 2001; Pickart, 2001; Bonifacino and Traub, 2003).

Many ubiquitinated proteins are recognized by domains that specifically bind to mono- and/or polyubiquitin. These include the UEV, UBA, UIM, and CUE domains or motifs (reviewed in Buchberger, 2002). The UEV domain is a counterpart of a ubiquitin-conjugating enzyme, as illustrated by the structure of the enzymatically inactive TSG101 UEV domain (Pornillos et al., 2002). The other three prominent ubiquitin binding domains, UBA, UIM, and CUE, are all small (20–50 amino acids) and are known or predicted to be α-helical. The ubiquitin binding UBA domain is found in DNA damage-inducible and other proteins (Hofmann and Bucher, 1996). UBA domains are three-helix bundles (Dieckmann et al., 1998; Withers-Ward et al., 2000; Mueller and Feigon, 2002) that can bind polyubiquitin with high affinity, and their physiological functioning is in at least some cases mediated by polyubiquitin binding (Wilkinson et al., 2001; Funakoshi et al., 2002). UBA domains also bind monoubiquitin (Vadlamudi et al., 1996; Bertolaet et al., 2001b; Chen et al., 2001), bind to other proteins (Dieckmann et al., 1998; Withers-Ward et al., 2000), and form homo- and heterodimers with each other (Bertolaet et al., 2001a). The UIM (ubiquitin interaction motif; Hofmann and Falquet, 2001) is a ubiquitin binding motif discovered in the proteasome subunit S5a. The S5a UIM binds polyubiquitin, but not monoubiquitin (Deveraux et al., 1994). In contrast, UIMs of many endocytic proteins bind monoubiquitinated proteins. The endocytic proteins epsin, eps15, Vps27p/Hrs, and Hse1p contain UIMs that bind monoubiquitin (Bilodeau et al., 2002; Klapisz et al., 2002; Oldham et al., 2002; Polo et al., 2002; Raiborg et al., 2002; Shih et al., 2002; Shekhtman and Cowburn, 2002). The UIMs of eps15 are essential for the ubiquitination of eps15 itself, representing a second function for UIMs in promoting the ubiquitination of proteins that contain them (Polo et al., 2002).

The most recent addition to the family of ubiquitin binding domains is the *c*oupling of *u*biquitin conjugation to *E*R degradation (CUE) domain, which is found in roughly 50 different proteins (Ponting, 2000, 2002; Bateman et al., 2002). CUE domains are named for the yeast Cue1p protein, which recruits the ubiquitin-conjugating enzyme Ubc7p to the ER, where it is essential for misfolded protein degradation (Biederer et al., 1997). Other CUE domain proteins include the autocrine motility factor receptor (AMFR), a ubiquitin protein ligase also involved in protein degradation at the ER (Fang et al.,

*Correspondence: james.hurley@nih.gov
[3]These authors contributed equally to this work.
[4]Present address: Laboratory of Biochemistry, National Cancer Institute, Bethesda, Maryland 20892.

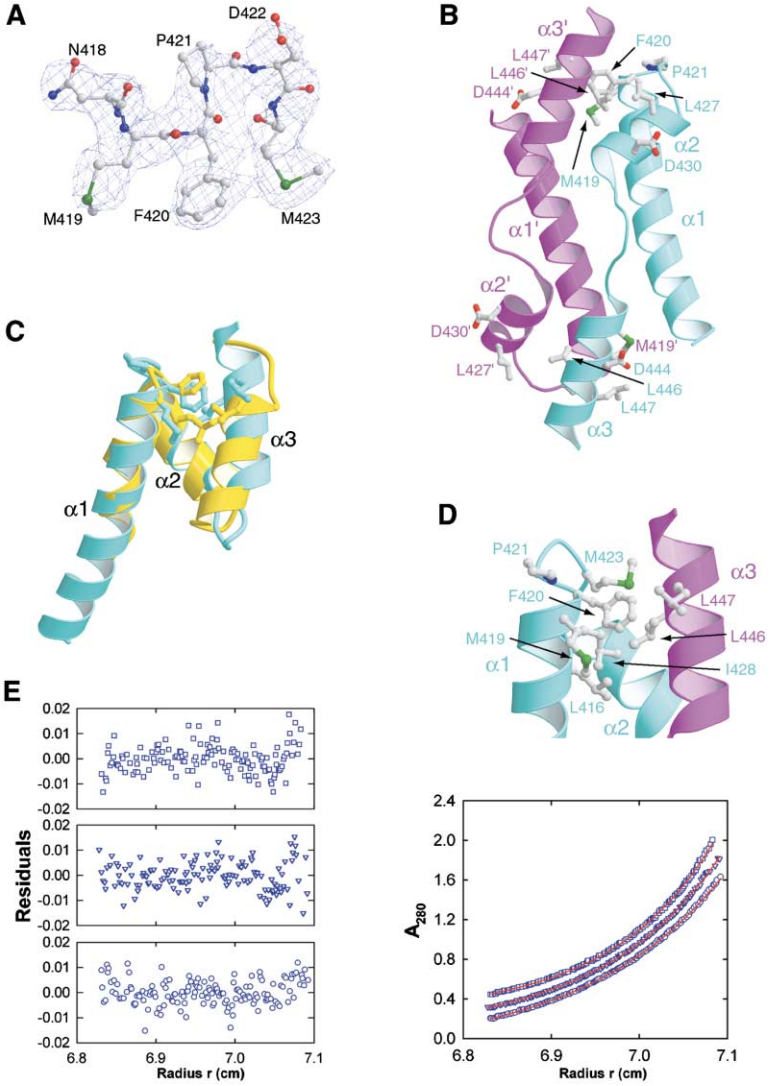

Figure 1. Structure of the Apo CUE Domain Dimer

(A) Refined CUE domain model, shown with solvent-modified density map contoured at 1.3 σ.

(B) The CUE domain fold. Residues mutated in the study are shown.

(C) Superimposition of the closed monomer CUE model and the hRad23-UBA(2) domain.

(D) Model of the closed CUE monomer in solution.

(E) Sedimentation equilibrium profiles at 280 nm and 20.0°C for Vps9p-CUE (left) at 24,000 (○), 26,000 (▽), and 28,000 (□) rpm. The red lines represent the best fit to a monomer-dimer equilibrium. The residuals to the fit are shown at left. Data at 24,000 rpm are shifted −0.2 A_{280} and at 28,000 rpm shifted by +0.2 A_{280}.

2001); Tollip, an interleukin-1 receptor-associated protein (Burns et al., 2000); Vps9p, a *Saccharomyces cerevisiae* exchange factor for the yeast Rab5 GTPase homolog Vps21p (Burd et al., 1996, Hama et al., 1999); Def1p, a Rad26-associated protein involved in ubiquitin-dependent proteolysis of RNA polymerase II (Ponting, 2002; Woudstra et al.., 2002), and enhancer trap locus-1 (Etl1).

The CUE domain of the sorting protein Vps9p binds directly to monoubiquitin (Shih et al., 2003; Donaldson et al., 2003; Davies et al., 2003) with an apparent K_d of 20 μM (Shih et al., 2003), regulates the endocytosis of the monoubiquitinated mating factor receptors Ste2p and Ste3p (Donaldson et al., 2003; Davies et al., 2003), and is essential for the ubiquitination in vivo of Vps9p (Shih et al., 2003; Davies et al., 2003). The CUE domain of Vps9p resembles the UIMs of eps15 in that it promotes ubiquitination within the same polypeptide chain. Other CUE domains bind to monoubiquitin, but some, such as that of Cue1p, bind with much lower affinity (Shih et al., 2003). The CUE domain is characterized by two conserved motifs, MFP and LL, that are essential for high-affinity binding to ubiquitin (Shih et al., 2003).

Little is known about mechanisms of ubiquitin recognition by the downstream effectors of ubiquitin signaling, and no structures of ubiquitin complexed to ubiquitin binding domains have been reported. The mechanism of discrimination between mono- and polyubiquitin is unknown. In order to shed light on this mechanism, we have obtained the crystal structure of the CUE domain of Vps9p alone and in complex with ubiquitin. On the basis of these structures and their functional analysis, we propose a mechanism for the differential recognition of monoubiquitin and polyubiquitin.

Results and Discussion

The Vps9p CUE Domain Is a Helical Dimer

The structure of the G440E mutant of the CUE domain of Vps9p (residues 394–451) was determined by multiwavelength anomalous dispersion (MAD) using the signal from the two SeMet residues and refined at 2.3 Å resolution (Figure 1A and Table 1). The G440E mutation was obtained as an artifact of the PCR reaction used to subclone the CUE domain into the protein expression

Table 1. Crystallographic Data, Phasing, and Refinement Statistics

Data Collection and Phasing			
	Apo	Complex Set 1	Complex Set 2
Space group	$P6_522$	C2	C2
Unit cell (Å)	a = b = 70.49 c = 61.38 $\alpha = \beta = 90^\circ$ $\gamma = 120^\circ$	a = 102.31 b = 46.69 c = 58.36 $\alpha = \gamma = 90$ $\beta = 97.33$	a = 101.61 b = 45.89 c = 57.80 $\alpha = \gamma = 90$ $\beta = 96.53$
Wavelength (Å)[a]	0.97910	0.9792	0.9564
Resolution (Å)	50–2.3 (2.38–2.3)[b]	50–2.2 (2.28–2.2)	50–1.7 (1.76–1.7)
Unique reflections	4327 (415)	13877 (1272)	28955 (2626)
Completeness (%)	99.8 (99.8)	98.7 (92.0)	98.4 (89.6)
Redundancy	23.5	6.8	3.5
$<I>/<\sigma>$	35.6 (6.2)	26.1 (5.9)	29.5 (2.3)
R_{merge}[c] (%)	8.6 (40.8)	7.2 (28.5)	4.0 (36.7)
Anom. differences (%)	4.3–5.9	3.2–4.7	
Disp. differences (%)	2.3–4.8	1.6–2.8	
FOM – SOLVE	0.43 (0.13)	0.42 (0.31)	
FOM – RESOLVE	0.57 (0.17)	0.49 (0.32)	

Refinement	Apo	Complex
Resolution range (Å)	43.4–2.30	50–1.7
No. of reflections	7325	55378
R[d] (%)	24.4	26.0
R_{free}[e] (%)	26.6	27.7
Cross validated Luzatti error	0.39	0.27
Rms deviations		
Bond length (Å)	0.006	0.01
Bond angle (°)	1.10	1.50
Improper angle (°)	0.86	1.06
Dihedral (°)	18.4	23.8
Average B factor (Å^2)	42.2	29.1
Protein atoms	425	1771
Solvent atoms	31	180
Residues in core ϕ–Ψ region	100%	99.5

[a] Statistics are shown for the peak wavelength of the Selenomethionine MAD datasets. Statistics for the inflection wavelength (0.97924 Å for apo and 0.97931 for complex) and remote wavelength (0.95645 Å for apo and complex) were very similar.
[b] Statistics in parentheses are for the highest resolution shell (Å).
[c] $R_{merge} = \Sigma|I(k) - <I(k)>|/\Sigma I(k)$.
[d] $R = \Sigma|F_{obs} - kF_{calc}|/\Sigma|F_{obs}|$.
[e] R_{free} is the R value calculated for a test set of reflections, comprising a randomly selected 10% of the data, not used during refinement.

vector and has little effect on the interaction with ubiquitin (Table 2). Residues 394–397, which precede the N terminus of the CUE domain as defined by Ponting (2000), are disordered.

The structure consists of three α helices and two connecting loops (Figure 1B). Helices α2 and α3 are antiparallel to the longer helix α1. The Vps9p CUE domain forms extensive dimer contacts across a crystallographic two-

Table 2. Mutational Analysis of CUE Function

Sample	Interface[1]	Apparent K_d (μM)[2]	Ubiquitination[3]	Puncta per Cell[4]
Vps9-CUE wild-type		20 ± 1	100	3.0 ± 1.7
M419D	mono/dimer	NB	12	7.9 ± 2.3
F420D	mono/dimer	NB	11	8.0 ± 2.8
L427D	dimer	171 ± 14	8	8.9 ± 2.6
D430A	dimer	71 ± 8	64	4.8 ± 2.5
K435A/K436A	dimer	60 ± 6	ND	ND
G440E	dimer	26 ± 2	ND	ND
C442T	none	34 ± 1	ND	ND
V443D	mono/dimer	ND	9	8.3 ± 2.8
D444A	mono/dimer	61 ± 6	65	6.6 ± 2.4
L447E	mono/dimer	133 ± 8	29	8.1 ± 2.5

[1] Mono/dimer indicates mutants that are in the α1/α3′ interface common to the monomer and dimer; dimer indicates mutants that are in the α2′ interface unique to the dimer; none, C442T is a control mutant for disulfide formation and not directly part of an interface.
[2] ITC measurements. NB, no detectable binding within a limit of ~500 μM; ND, not determined.
[3] Percent wild-type in vivo ubiquitination levels, quantified with a UVP bioimaging system.
[4] >50 cells scored per data point.

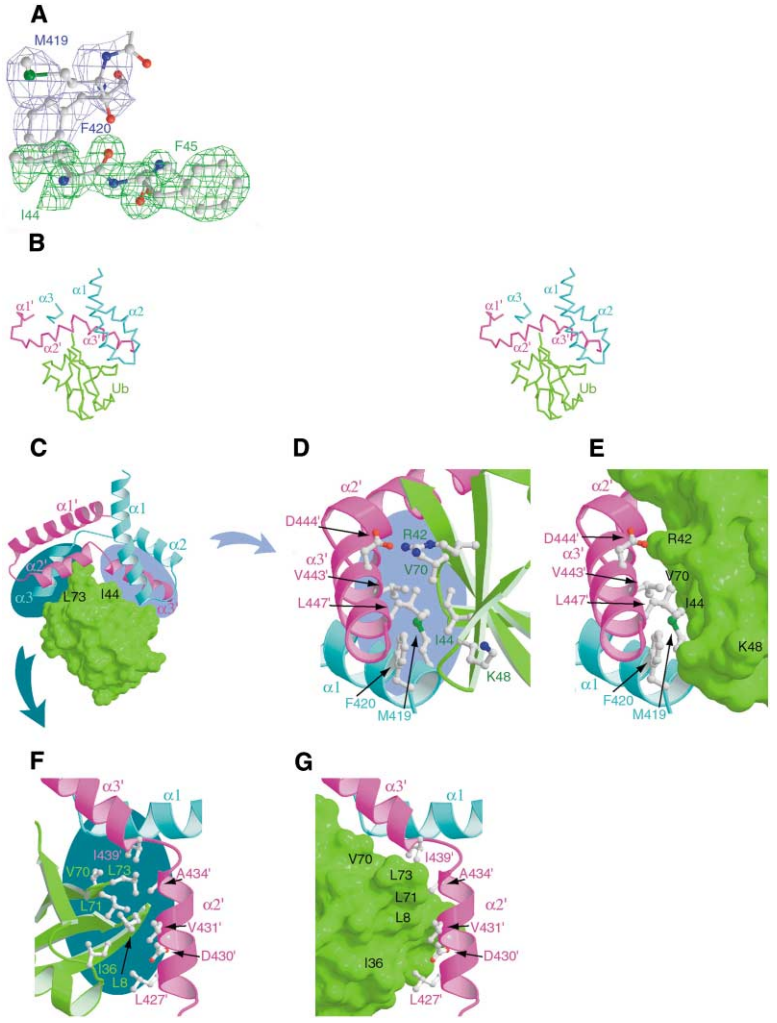

Figure 2. Structure of the CUE Dimer:Ubiquitin Complex

Only the ubiquitin making functionally relevant contacts with the CUE dimer is shown. (A) Refined CUE:ubiquitin complex model, shown with the solvent-modified experimental map contoured at 1.5 σ. (B) Stereo view of a Cα trace of the backbone; ubiquitin is green, and well-ordered parts of the CUE chains are red and blue. (C) Ribbon drawing of a model of the complex. The disordered regions of the CUE dimer in the complex were modeled by overlaying the separate chains of the apo CUE dimer on the complex conformation of the CUE dimer. Closeup of the interaction between CUE and ubiquitin in the α1/α3′ interface (D and E) and the α2′ interface (F and G), with selected side chains shown, and backbones and surfaces colored as in (B).

fold axis (Figure 1B). Helix α3 of one monomer nestles between α1 and α2 of its symmetry-related mate. The interface buries 780 Å^2 of solvent-accessible surface area from each monomer. The dimer in the crystal is bridged by disulfide bonds between Cys-432 and Cys-442.

Sedimentation equilibrium centrifugation was used to determine whether Vps9p-CUE is a dimer in solution. An excellent fit was obtained to a reversible monomer-dimer equilibrium (Figure 1E) with a K_d (dimerization) of 1 mM. The mutation C442T was engineered to prevent intermolecular disulfide bond formation and has near wild-type affinity for ubiquitin (Table 2). The sedimentation behavior of the C442T mutant was identical to that of wild-type (data not shown), indicating that the dimer is not an artifact of oxidation.

A UBA-like Fold for the CUE Domain

Despite negligible sequence identity (17% with Rad23 UBA[1]), the CUE domain structure revealed significant structural homology with the UBA domain. The first two helices of the apo CUE domain can be superimposed on the corresponding helices of the UBA domains of Rad23 (Figure 1C). The rmsd for 22 Cα positions (excluding α3) is 2.1 Å for the CUE domain with Rad23-UBA(1) and 1.8 Å for Rad23-UBA(2). The UBA domains have a hydrophobic motif ΦGAr (where Φ is hydrophobic and Ar is aromatic) at the end of α1 in the UBA structures (Figure 1C) that coincides with the critical MFP motif of the CUE domain (Figure 1D). This hydrophobic site corresponds to the Vpr binding site in Rad23 UBA domains, as shown by NMR chemical shift perturbations (Dieckmann et al., 1998; Withers-Ward et al., 2000; Mueller and Feigon, 2002), and the ubiquitin binding site of the Rad23-UBA domain(s) as judged by mutational analysis (Bertolaet et al., 2001b). Taking the structural and functional similarities together, CUE and UBA can be grouped into a superfamily of three-helical ubiquitin binding domains.

The Vps9p CUE Domain Dimerizes by Domain Swapping

The α3 helix of one CUE monomer interacts with α1 and α2 of its partner using interactions equivalent to those of α3 of the UBA monomer with α1 and α2. The CUE domain undergoes a monomer:dimer equilibrium in solution. We assume that in solution, the unliganded CUE monomer is in a closed, globular conformation similar to the UBA domain. We have modeled the structure of

this closed monomer, assuming that the observed dimer is the product of domain swapping (Liu and Eisenberg, 2002), in which the two monomers have exchanged their α3 helices. The model was constructed using the program Swiss-Pdb Viewer (Guex and Peitsch, 1997). The loop connecting helices 2 and 3 of one monomer was deleted and rebuilt to connect helix 2 of one monomer and helix 3 of the other. In this model, all three helices of the CUE and UBA domains are superimposable (Figure 1C). The hydrophobic core packing interactions in the closed CUE monomer and UBA cores are equivalent (Figure 1D). Domain-swapped oligomers such as CUE that do not have a known closed monomer structure but do have a homolog with a closed monomer structure are classified as quasi-domain swapped (Liu and Eisenberg, 2001).

Structure of the CUE Dimer:Ubiquitin Complex

The structure of the K435A/K436A mutant of the Vps9p-CUE domain in complex with ubiquitin was determined by MAD phasing from SeMet CUE protein crystallized in complex with native bovine ubiquitin and refined to a resolution of 1.7 Å (Figure 2A, Table 1). The K435A/K436A mutant binds ubiquitin (Table 2) and was engineered using the strategy of Derewenda and coworkers (Longenecker et al., 2001) to facilitate crystallization of the Vps9p-CUE complex after crystallization of the wild-type complex failed.

The crystallized complex contains two ubiquitin molecules and two CUE domains per asymmetric unit. The two ubiquitin molecules are well ordered, with the exception of two and three mobile residues in their respective C termini. The two molecules are superimposable on the structure of ubiquitin crystallized alone with rmsd values of 1.1 and 0.9 Å for all Cα positions (Vijay-Kumar et al., 1987; pdb entry 1ubq). One of the CUE domain monomers is ordered from residues 408–437 and partially ordered in residues 440–444 (Figure 2B). The second CUE monomer is ordered from 416′–451′, where the prime (′) indicates the second CUE chain. There are residual positive difference density features in Fo-Fc syntheses that are uninterpretable as an atomic model but probably represent partially disordered regions. These features may explain the relatively high free R factor (Table 1). The Vps9p CUE domain in the crystallized complex is a domain-swapped dimer, but the ubiquitin-bound CUE dimer is not disulfide bonded.

The bound CUE dimer undergoes a dramatic conformational change (Figure 3) relative to the apo structure. Residues 398–431 and 437′–451′ belong to a rigid core that shifts by only 1.2 Å rmsd (Cα positions). With these residues used for reference, α3 moves 28 Å (Cα of 444), and the N terminus of α2′ moves 21 Å (Cα of 424). Residues 434–437 form an extended coil that pivots to allow a large movement between α2 and α3. The entire α1′/α2′ unit rotates by roughly 180° relative to its orientation in the apo structure. The conformational changes in the CUE dimer bend it 122° into the rod-like apo structure, pushing it into the shape of a basket with an opening 36 Å across, 16 Å wide, and 8 Å deep.

The CUE dimer wraps itself partway around one of the two ubiquitin molecules in the asymmetric unit (Figures 2B and 2C). The interface buries 654 Å^2 of solvent-accessible surface area each from the ubiquitin and the CUE dimer. The CUE domain binds to a hydrophobic patch on ubiquitin defined by Leu-8, Ile-44, and Val-70 identified as a binding site for the proteasome, UIMs, and UBA domains (Beal et al., 1996; Shih et al., 2000; Sloper-Mould et al., 2001; Shih et al., 2002). Ile-44 was shown by mutational analysis to bind to the Vps9p CUE domain (Shih et al., 2003), consistent with our structural observations.

The first highly conserved motif is the sequence MFP (residues 419–421) in Vps9p-CUE (Figure 4). Met-419 and Phe-420 directly bind to ubiquitin residues Ile-44, Ala-46, Gly-47, His-68, Leu-69, and Val-70 (Figures 2D and 2E). Pro-421 serves as a helix-breaker at the end of α1, and contacts Ala-46 and Gly-47 of ubiquitin. The C-terminal conserved motif in the CUE domain consists of ϕxx (I/L/V)L, where ϕ is a large hydrophobic residue. In Vps9p, the first position ϕ corresponds to Val-443′, and the latter two positions correspond to Leu-446′ and Leu-447′. Val-443′ interacts with ubiquitin Arg-42, Ile-44, and Val-70. Leu-447′ interacts with ubiquitin Arg-42, Gly-47, Lys-48, and Gln-49. Leu-446′ is buried in the center of the hydrophobic core and is required for stability, rather than binding. A salt bridge is formed between Glu-444′ and ubiquitin Arg-42, and there is a hydrogen bond between Asn-418 and His-68.

The MFP and C-terminal conserved motifs bind the same surface of ubiquitin, surrounding Ile-44, but the third conserved motif interacts with the opposite side of the interface, around Leu-8, Ile-36, and Leu-73 (Figures 2F and 2G). In the CUE domains, the central portion of the α2 helix contains the conserved sequence (I/L/V)xxxL. The first conserved position in this sequence corresponds to Ile-428 in Vps9p. Ile-428 is a key residue in the α1/α2 packing interface, making contact with Leu-413 and Leu-416 on α1. The second conserved position, which is a Leu in nearly all other CUE domains, is occupied by Cys-432 in Vps9p. In the CUE dimer complex, ubiquitin interacts with α2′. The two strongest hydrophobic interactions in this site are made by Leu-427′ and Val-431′. Leu-427′ interacts with ubiquitin Glu-34, Gly-35, and Ile-36, while Val-431′ interacts with Leu-71. Additional hydrophobic contacts in this site are made between Ile-433′ and ubiquitin Leu-8, and between Ala-434′ and Leu-71. The Cβ of Ala-435′, which replaces Lys-435 in wild-type, makes contact with Leu-73. The aliphatic moiety of the Lys side chain in wild-type is predicted to make more extensive interactions. The loss of these interactions would explain the reduced affinity of K435A/K436A for ubiquitin (Table 2, Figure 5A). Asp-430′ interacts with Thr-9. The α2′ contact residues are less conserved than the MFP and LL motifs, so this contact may be a feature of the high-affinity monoubiquitin binding subclass of CUE domains, rather than all CUE domains.

The last contact region is formed by part of the linker between the domain-swapped monomers (residues 438′–440′). The side chain of Arg-438′ approaches the C terminus of the ordered part of ubiquitin at Leu-73. Ile-439′ makes a hydrophobic contact with Val-70, and Gly-440′ contacts Arg-42 and Val-70. The domain-swapped conformation allows this linker region to wrap halfway around the C terminus of ubiquitin.

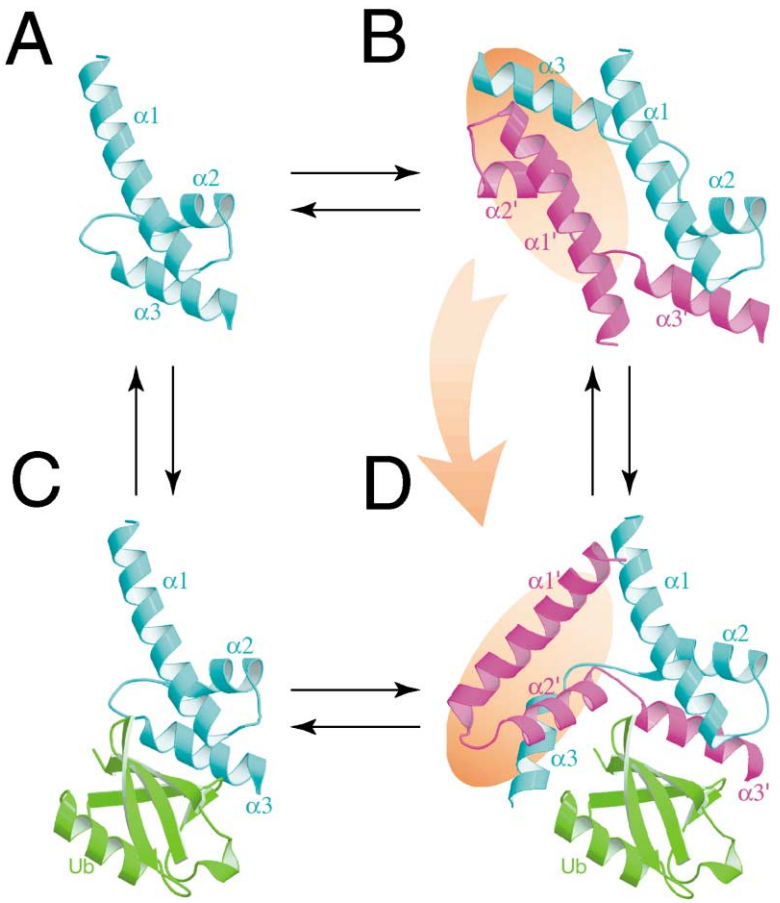

Figure 3. Conformational Changes in the CUE Domain

(A) Closed monomer model of the Vps9p CUE domain derived from the domain-swapped dimer.

(B) Apo CUE domain dimer.

(C) Closed monomer model bound to ubiquitin.

(D) Model of the CUE dimer bound to ubiquitin, with disordered regions modeled as in Figure 2. The orange oval in the background in (B) and (D) is intended to guide the eye through the conformational change.

The CUE Dimer Interface Is Required for High-Affinity Ubiquitin Binding

To determine the relative contributions of the CUE monomer and dimer to ubiquitin binding, we modeled the interaction of ubiquitin with a closed CUE monomer (Figure 3A). The CUE monomer can interact with ubiquitin through α1 and α3, which contain the MFP motif (Met-419 and Phe-420) and the LL motif (Leu-447). The monomer interface also includes Val-443 and Asp-444. The surface of α2, which includes Leu-427, Asp-430, and Val-431, is on the side of the CUE monomer that faces away from ubiquitin and has no interactions with it. Several ubiquitin hydrophobic residues (e.g., Leu-8 and Leu-73) that are functionally important in ubiquitin-dependent internalization (Sloper-Mould et al., 2001) make no contact with the monomer. These residues are only buried in the dimer interface. The monomer buries 419 Å^2 of solvent-accessible surface area from each partner.

Mutations were constructed to test which of the two faces of the CUE domain were involved. Several mutants were made in which surface hydrophobic residues were replaced with acidic residues. The mutant proteins M419D, F420D, L427D, D430A, D444A, and L447E were stable enough to be expressed and purified at wild-type levels. The interactions between all of these mutant proteins and ubiquitin were measured by isothermal titration calorimetry (ITC). The α1/α3′ interface mutants M419D and F420D had undetectable binding by ITC (Table 2, Figure 5A). The two other mutants in α1/α3′ interface residues, D444A and L447E, reduced, but did not abolish, binding. Mutants in the α2′ interface, L427D and D430A, both reduced binding. The hydrophobic mutant L427D produced the strongest effect, a nearly 10-fold reduction in affinity.

The mutational analysis shows that both interaction surfaces of the CUE domain are required for strong binding to ubiquitin. The most disruptive mutations in the α1/α3′ interface abolish binding completely. This is consistent with the conservation of these residues and previous mutational analysis. This finding rules out the binding of a CUE monomer to ubiquitin via α2 of the monomer, since in this model, the MFP and LL motifs do not contact ubiquitin. Disruption of the α2′ interface reduces binding by roughly 10-fold. This finding leads us to conclude that a CUE monomer is capable of binding to ubiquitin via an interface formed by its α1 and α3 helices. It also sets an upper limit of ~170 μM to the affinity of the monomer for ubiquitin. The low affinity of the monomer for ubiquitin is consistent with the small amount of solvent-accessible surface area buried in the interface. Because disruption of either interface greatly impairs or abolishes ubiquitin binding, we conclude that both interfaces are required for high-affinity binding. The surface area buried in the combined interface is consistent with the high affinity of CUE for ubiquitin determined from sedimentation analysis (see below).

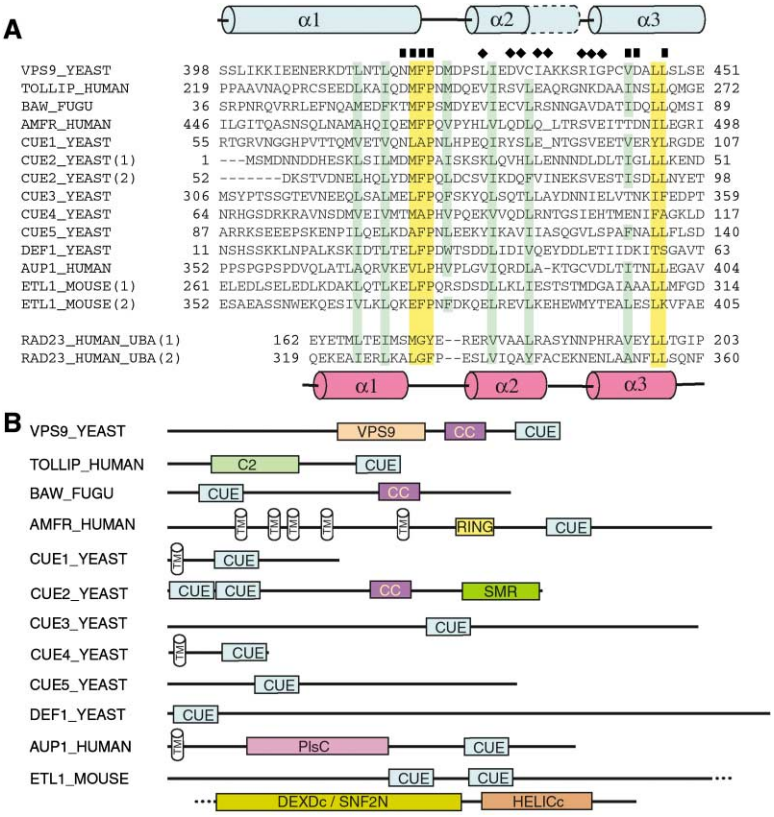

Figure 4. Conservation of CUE Domains

(A) Alignment of representative CUE domains and the two UBA domains of human Rad23. Contact residues that interact in both the monomer and dimer are marked with rectangles above them; residues that only interact in the dimer, small diamonds. Core hydrophobic residues of the CUE domains are highlighted in green; conserved MFP and LL motifs that bind ubiquitin, in yellow. Sequences are as described, with the addition of BAW, the Fugu homolog of the neurofibromatosis-1 protein, and AUP1, the ancient ubiquitous protein-1 (Ponting, 2000). The terminology for CUE2–5 follows Shih et al. (2003). The secondary structures are derived from the apo structure. The α2′ helix of the complexed dimer is longer than α2 in the apo structure, and the additional length of α2′ is shown in dashed lines. (B) Other domains found in the CUE-domain-containing proteins in (A): VPS9, Vps9p-homology domain; C2, protein kinase C homology-2 domain; CC, coiled coil; TM, transmembrane helix; RING, zinc-finger/E3 ubiquitin protein ligase domain; SMR, small mutation S related protein homology domain; PlsC, phospholipids acyltransferase catalytic domain in Taffazin; DEXDc, DEXD helicase catalytic domain; HELICc, helicase C-terminal domain.

Both interfaces can be presented to a single ubiquitin molecule in the dimer, but not in the monomer. The only reasonable explanation for the mutational data is that the CUE monomer is capable of binding ubiquitin with low affinity, but the dimer is the only form of the CUE domain capable of binding with high affinity.

The Vps9p CUE Domain Functions as a Dimer In Vivo

In order to assess the role of the CUE dimer interface in vivo, the CUE interface mutants were incorporated into intact Vps9p and assessed in vivo in yeast (Figures 5B and 5C). One function of the Vps9p CUE is to promote ubiquitination of Vps9p itself (Davies et al., 2003; Shih et al., 2003). Mutations in the interface common to both the monomer and dimer either blocked (M419D, F420D, V443D) or reduced (D444A, L447E) ubiquitination. Mutations in the α2 interface, which is only formed in the dimer, either completely blocked (L427D) or sharply reduced (D430A) ubiquitination. The rank order of the effects of the mutants on ubiquitination in vivo and direct binding in vitro are nearly identical (Table 2). The Vps9p-CUE is required for the efficient endocytosis of the mating factor receptor Ste3p. Analysis of a Ste3-GFP reporter indicated a partial defect in Ste3p trafficking with the increased appearance of perivacuolar pucta in yeast expressing Vps9 alleles bearing the CUE domain mutations described above (Table 2; Figure 5C). Mutations at either the monomer/dimer common ubiquitin binding interface or the unique ubiquitin binding interface of the dimer interfere withVps9p function in vivo to similar degrees. Thus the entire ubiquitin binding interface of the CUE domain dimer is required for in vivo function, not just the portion of the interface present in the CUE monomer.

We tested whether Vps9p-CUE was capable of dimerizing in vivo and whether interactions between other portions of Vps9p could affect the stability of the dimer in vivo using the yeast two-hybrid system (Figure 5D). A collection of bait and prey fusions were constructed that expressed various portions of Vps9p, and interaction was scored using a β-galactosidase reporter system (see Experimental Procedures). Prey fusions that encoded full-length Vps9p (residues 1–451) interacted with a bait fusion that encoded the C-terminal portion of Vps9p (residues 159–451) and a bait fusion that encoded only the Vps9 CUE domain (residues 408–451). Additionally, the bait fusion containing only the CUE domain also interacted with a prey fusion that contained only the CUE domain, indicating that the CUE domain robustly interacted with itself in vivo. These results support the conclusion that the Vps9p CUE domain dimerizes in vivo.

Quantitation of CUE Monomer and Dimer Complexes with Ubiquitin in Solution

We sought to determine whether ubiquitin complexes with monomers and dimers could be detected in solution using sedimentation equilibrium centrifugation. To test the role of the dimer interface in complex formation, studies were executed in parallel on wild-type and on the α2 interface mutant L427D. The L427D mutant was predicted to destabilize the ubiquitin complex with the CUE dimer, but not with the CUE monomer. In order to

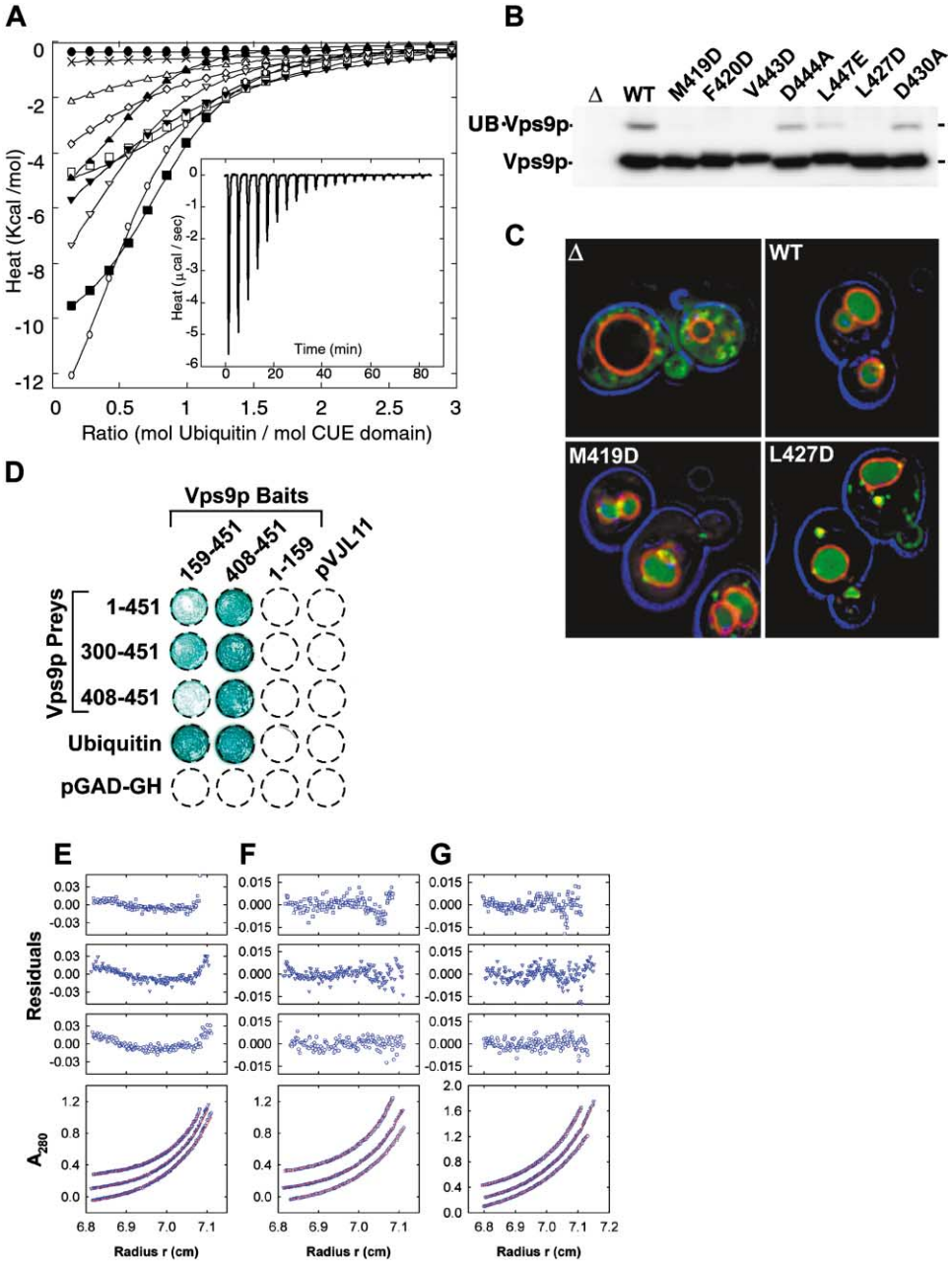

Figure 5. Functional Analysis of the CUE Dimer

(A) ITC titration curves for: ■, wild-type; ×, M419D; ●, F420D; △, L427D; ◇, D430A; □, K435A, K436A; ▲, G440E; ○, C442T; ▽, D444A; and ▼, L447E. Inset: representative experimental ITC trace. The differential heat signal from injection of 4.0 mM ubiquitin into 200 μM wild-type Vps9p CUE domain is shown (after subtraction of data from injection of ubiquitin into a buffer blank).

(B) Lysates were generated from Δvps9 (lane 1) and Δvps9 yeast strains expressing wild-type and mutant alleles encoded on a plasmid. Western analysis with Vps9p antiserum was performed, and the sizes of the unmodified and ubiquitinated forms of Vps9p are indicated.

(C) Microscopic analysis of Ste3-GFP (green) in ΔVps9 (Δ) and ΔVps9 yeast strains expressing wild-type (WT), L427D, or M419D alleles. The vacuolar limiting membrane is labeled with FM4-64 (red), and the perimeter of the cell was visualized with blue light.

(D) L40 yeast that were cotransformed with the indicated bait and prey plasmids were grown on selective media, transferred to a nitrocellulose, lysed, and the presence of β-galactosidase was determined using a colorimetric filter assay.

(E–G) Sedimentation equilibrium profiles at 280 nm and 20.0°C. (E) A 1:1 mixture of CUE and ubiquitin fit to a noncooperative interaction (equation [2]), illustrating that wild-type CUE is not properly fit by this model. (F) A 2:1 mixture of CUE and ubiquitin fit to a cooperative interaction (equation [1]). (G) A 1:1 mixture of L427D CUE and ubiquitin fit to a noncooperative interaction (equation [2]). Symbols correspond to data collected at 24,000 (circles, shifted by −0.2 A280), 26,000 (▽), and 28,000 (□, shifted by +0.2 A280) rpm.

model the data without overfitting, two simplified models were constructed. In one model, the interactions in the dimer are cooperative and in the other, they are noncooperative. Both models contain only one adjustable parameter, K_0, which represents the association constant for the formation of a 1:1 CUE:ubiquitin com-

plex (CU). In the cooperative model, the CUE dimer interacts with ubiquitin in only one manner such that the free energy of this 2:1 complex formation is twice that for 1:1 complex formation. In the noncooperative model, the free energies of formation of the C_2U and U_2C complexes from the CUE dimer and free ubiquitin are identical to that for 1:1 complex formation. Data for the wild-type CUE did not fit the noncooperative model (Figure 5E), but excellent fits to the cooperative model were obtained (Figure 5F). The fit to the data yields a wild-type CUE dimer:ubiquitin K_d value of 1.2 μM (within error, 0.5–3.0 μM) and a wild-type monomer:ubiquitin K_d value of 1.1 mM (within error, 0.7–1.9 mM). Complexes with the L427D CUE:ubiquitin mixture gave an excellent fit to the noncooperative model (Figure 5G), with a CUE:ubiquitin K_d value of 3 mM (within error, 2–4 mM); the K_d values for the L427D mutant monomer and dimer are identical given the noncooperative nature of the model. The low $\sim$1 mM affinity of the CUE monomer agrees well with the limit of $>$170 μM derived from ITC of mutants. The high $\sim$1 μM affinity of the Vps9p CUE dimer for a single ubiquitin monomer would be consistent with a physiological function for the dimer in monoubiquitin recognition.

Lattice Contacts Explain Multiple Binding Modes

The presence of two ubiquitin monomers per CUE dimer in the crystal was surprising, since the CUE dimer wraps around only one of the two ubiquitin molecules. Lattice contacts with the other ubiquitin molecule show that the same residues that make specific contacts with the primary ubiquitin are used by the second ubiquitin molecule to hold the crystal lattice together. The hydrophobic surface surrounding Leu-8, Ile-44, and Val-70 of the second ubiquitin molecule forms lattice contacts with the convex "back" sides of two different CUE dimers in the crystal (Figure 6). Each CUE dimer has two "left-over" hydrophobic contact sites that do not interact with the primary ubiquitin. Because the CUE dimer is bent to wrap around the primary ubiquitin molecule in a concave manner, the side of the CUE dimer opposite to the primary ubiquitin contact is convex in shape. The convex shape makes it impossible for the back side of the dimer to wrap around a second ubiquitin. The Ile-44 region of the second ubiquitin contacts the dimer-related α2 surface of one CUE dimer, burying 608 Å^2 of solvent-accessible surface area. The Ile-36/Leu-73 region of the same ubiquitin molecule contacts the dimer-related α1′/α3 interface of a different CUE dimer in the crystal lattice, burying 263 Å^2 of solvent-accessible surface area. Taken together, the two separate surfaces on the back sides of two separate lattice-related CUE dimers form a hydrophobic basket. The basket is a remarkable mimic of the primary ubiquitin binding site on front side of a single CUE dimer, except that the pattern of intermolecular contacts is inverted (Figure 6F).

The lattice contacts between CUE domains and ubiquitin explain the mixture of species observed in the sedimentation equilibrium experiments. Binding of the CUE dimer to ubiquitin occupies the concave high-affinity interaction surface. However, the dimer-related MFP and LL surface and the dimer-related α2 surface are exposed and can interact with additional ubiquitin molecules with low affinity. These interactions give rise to

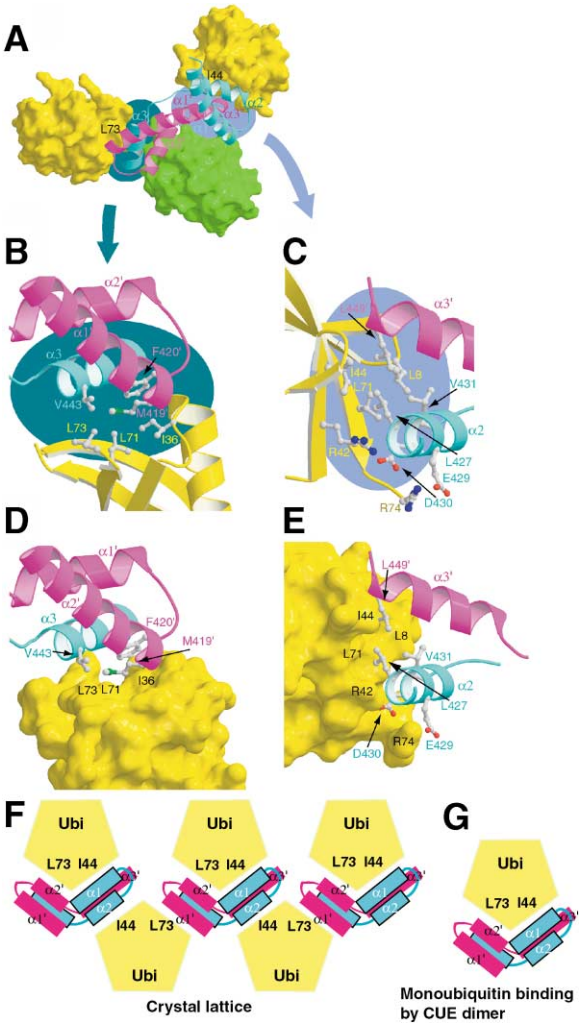

Figure 6. Multivalent Interactions in the Crystal and Model for Monoubiquitin Binding

(A) A CUE domain dimer interacting with its primary ubiquitin binding partner (center) and two lattice-related ubiquitin molecules. Closeup views of the molecular contacts are shown for the interaction between CUE α1′/α 3 and ubiquitin Ile-44 region (light blue oval, [B] and [D]), and the CUE α2 and ubiquitin Ile-36/Ile-73 region (teal oval, [C] and [E]). (F) Schematic illustration of the lattice relationships. (G) Schematic of the high-affinity ubiquitin binding mode of the CUE dimer.

the 1:1 CUE:ubiquitin stoichiometry in the crystal, the apparent 1:1 binding of CUE to ubiquitin by ITC, and the presence of 2:2 complexes in solution as judged by the sedimentation equilibrium analysis. The presence of multiple complexes in solution explains why the CUE (monomer + dimer):ubiquitin K_d value of 20 μM obtained by ITC is higher than the CUE dimer:ubiquitin K_d obtained by fitting the sedimentation data. The heat released in the ITC experiment represents all binding modes, while the sedimentation analysis treats binding of the CUE monomer and dimer as separate events.

Mechanism for Recognition of Monoubiquitin and Polyubiquitin

It is widely believed that monoubiquitin recognition is a physiological function of the Vps9p-CUE domain. Never-

theless, Vps9p-CUE also binds polyubiquitin in vitro (Shih et al., 2003). Since the terminal ubiquitin in a polyubiquitin chain is equivalent to a monoubiquitin modification, monoubiquitin binding domains must bind polyubiquitin. The converse does not apply, since a ubiquitin monomer offers fewer potential interaction surfaces than a polymer. The challenge in monoubiquitin recognition is for a targeting domain to achieve an affinity high enough to bind a monoubiquitinated protein at physiological concentrations.

The structural analysis shows how different members of a family of related domains could interact with either mono- or polyubiquitin, using the same underlying molecular interfaces in different oligomerization states. Dimerization of the CUE domain allows both interaction surfaces of the CUE domain to be presented simultaneously to a single ubiquitin monomer (Figure 6G). This leads to an extensive contact surface between the ubiquitin monomer and the CUE dimer that would not be possible if both molecules were monomers. This suggests an elegant hypothesis for mono- versus polyubiquitin recognition in which the molecular interactions are identical, and specificity is controlled by the dimerization states of the binding domain. Given the structural similarities of CUE to UBA and the functional similarity of CUE to UIM, it will be interesting to see if such a principle applies to these domains as well.

Experimental Procedures

Crystallization of the Vps9p-CUE Domain

The G440E mutant of the CUE domain of *S. cerevisiae* Vps9p was expressed and purified (Shih et al., 2003). SeMet G440E Vps9p CUE domain was expressed in *E. coli* strain B834 (DE3) and purified. The Vps9p CUE domain was concentrated to 30 mg/mL; dialyzed into 50 mM NaCl, 20 mM Tris (pH 7.7), and 10 mM DTT; and crystallized in 2 μl hanging drops over 0.5 ml reservoirs of 1.9–2.1 M ammonium sulfate and 100 mM Tris-HCl (pH 8.2–8.8). Crystals were cryoprotected in mother liquor supplemented with 25% ethylene glycol and frozen in liquid propane.

Crystallization of the Vps9p-CUE:Ubiquitin Complex

The Vps9p-CUE K435A/K436A mutant was mixed with bovine ubiquitin (Sigma) at a 1:1 molar ratio. The complex was isolated from unbound material on a Superdex 75/S60 gel filtration column (Pharmacia). Native protein was concentrated to 43 mg/ml and crystallized in the presence of 17% polyethylene glycol 3350 and 200 mM $MgCl_2$. SeMet CUE:ubiquitin crystals were obtained in similar conditions. Crystals of the complex were cryoprotected in mother liquor supplemented with 18% glycerol and frozen in liquid propane or in the cryostream.

Structure Determination

MAD data sets were collected from apo and ubiquitin bound CUE crystals at beamlines 19ID and 22ID, respectively, at the Advanced Photon Source, Argonne National Laboratory. MAD data were collected at three wavelengths, at 95 K, and in 1° oscillation frames, and reduced using DENZO and Scalepack (Otwinowski and Minor, 1997). Se atoms were located and phases were calculated with SOLVE (Terwilliger and Berendzen, 1999). Density modification of the initial maps was performed using RESOLVE (Terwilliger, 2000). The resulting maps were used to build atomic models in O (Jones et al., 1991). The models were initially refined using CNS (Brünger et al.,1998; Table 1). The complex model was subsequently refined at 1.7 Å using Refmac5 of the CCP4 suite programs (CCP4, 1994).

Site-Directed Mutagenesis

Site-directed Vps9p CUE domain mutants were constructed using the GeneTailor mutagenesis kit (Invitrogen) and confirmed by DNA sequencing.

Isothermal Titration Calorimetry

CUE domains and bovine ubiquitin (Sigma) were dialyzed against 100 mM NaCl, 50 mM Na/K phosphate buffer (pH 7.5), and 1 mM DTT. Protein concentrations were adjusted to 200 μM and 4.0 mM for CUE and ubiquitin, respectively. Measurements were performed on a MicroCal VP-ITC instrument at 30°C. Ubiquitin was injected into 1.4 ml of buffer containing CUE domain in 21 injections of 10 μl each. Traces were corrected by subtracting blank measurements and analyzed using Origin 5.0 (MicroCal). Binding constants were calculated by fitting the integrated titration data to a one-site binding model (Table 2).

Sedimentation Equilibrium

CUE, CUE-L427D, and ubiquitin in 150 mM NaCl, 50 mM Tris-HCl (pH 7.5), and 1 mM Tris (2-carboxylethyl) phosphine hydrochloride (TCEP) or 2- mercaptoethanol were loaded at 0.5–0.9 A_{280}. Mixtures containing 1:1 and 2:1 molar ratios of CUE:ubiquitin and CUE L427D:ubiquitin were loaded at 0.85 A_{280}. Experiments were conducted at 20.0°C and 280 nm on a Beckman Optima XL-A analytical ultracentrifuge at rotor speeds of 24,000, 26,000, and 28,000 rpm. Data for ubiquitin were analyzed as a single ideal solute to obtain the buoyant molecular mass, $M_1(1 - \nu_1\rho)$. Values of M_1 were calculated using densities obtained from standard tables and calculated values of ν_1 (Perkins, 1986). Sedimentation equilibrium data for CUE and CUE-L427D were analyzed as reversible monomer-dimer equilibria to obtain a dimerization equilibrium constant, K_{dim} (Jenkins, et al., 1996).

Data for the 1:1 and 2:1 mixtures of CUE:ubiquitin and CUE-L427D:ubiquitin were analyzed in terms of the following equilibria:

$$K_{dim}: C + C \rightleftharpoons C_2$$

$$K_0: C + U \rightleftharpoons CU$$

$$K_{01}: C_2 + U \rightleftharpoons C_2U$$

$$K_{10}: C_2 + U \rightleftharpoons UC_2$$

$$K_2: C_2U + U \rightleftharpoons C_2U_2,$$

where C and U are CUE and ubiquitin. Two models were considered. In the cooperative model, the cooperativity results in the exclusive formation of C_2U with $\Delta G_{01} = 2\Delta G_0$ or $K_{01} = K_1 = (K_0)^2$. In the noncooperative model, the complexes C_2U and UC_2 are symmetrically indistinguishable, with $K_{01} = K_{10} = K_0$ and $K_{01} + K_{10} = K_1$. In both models, it is assumed that $K_2 = K_0$. The model equations, values for the constants, and their error limits, are described in the online Supplemental Data, http://www.cell.com/cgi/content/full/113/5/609/DC1.

Strains, Reagents, and Plasmids for In Vivo Experiments

The *Saccharomyces cerevisiae* strains used were CBY1 (SEY6210; *vps9Δ1::HIS3*) (Burd et al., 1996) and BHY93, which was constructed by integrating pRS304 Ste3GFP (linearized with *Eco*RV) into CBY1. Reagents and plasmids used are described by Davies et al. (2003).

FM4-64 Labeling and Ste-GFP Localization Assay

Vacuolar morphology was analyzed by labeling with FM4-64 (Molecular Probes, Eugene, OR) as described (Vida and Emr, 1995), except that labeling was at a concentration of 16 μM at 30°C, cells were chased 1 hr, and cyclohexamide was added (3 μg/ml) during the last 45 min of the chase period. Labeled cells were visualized on an Olympus IX70 inverted microscope with a Rhodamine filter. Ste3-GFP was visualized with a FITC filter. Images were collected with a Photometrix digital camera and deconvolved using DeltaVision (Applied Precision).

Two-Hybrid Analysis

Yeast strain L40 (Vojtek, et al., 1993) was transformed with bait plasmid alone (pVJL11) (Jullien-Flores, et al., 1995) or with bait plasmids that also encoded the indicated portions of Vps9p. These transformants were cotransformed with the prey plasmid alone (pGAD-GH), or prey plasmids encoding full-length or the indicated portions of Vps9p, or a prey plasmid expressing ubiquitin. Cotransformants were selected on minimal media and interaction was scored using a β-galactosidase filter assay (Vojtek et al., 1993).

Acknowledgments

We thank B. Beach for DNA sequencing, A. Hickman for critical comments on the manuscript, G. Miller and R. Trievel for assistance with data collection, and A. Weissman for discussions. This study was supported in part by NIH grant number GM55301 to B.F.H. and a predoctoral fellowship from the HHMI to B.A.D. We acknowledge use of the SBC-CAT and SER-CAT beamlines at the APS, ANL. Use of the Advanced Photon Source was supported by the U.S. Department of Energy, Basic Energy Sciences, Office of Science, under Contract No.W-31-109-Eng-38.

Received: February 3, 2003
Revised: April 22, 2003
Accepted: April 29, 2003
Published: May 29, 2003

References

Bateman, A., Birney, E., Cerruti, L., Durbin, R., Etwiller, L., Eddy, S.R., Griffiths-Jones, S., Howe, K.L., Marshall, M., and Sonnhammer, E.L. (2002). The Pfam protein families database. Nucleic Acids Res. *30*, 276–280.

Beal, R., Deveraux, Q., Xia, G., Rechsteiner, M., and Pickart, C. (1996). Surface hydrophobic residues of multiubiquitin chains essential for proteolytic targeting. Proc. Natl. Acad. Sci. USA *93*, 861–866.

Bertolaet, B.L., Clarke, D.J., Wolff, M., Watson, M.H., Henze, M., Divita, G., and Reed, S.I. (2001a). UBA domains mediate protein-protein interactions between two DNA damage-inducible proteins. J. Mol. Biol. *313*, 955–963.

Bertolaet, B.L., Clarke, D.J., Wolff, M., Watson, M.H., Henze, M., Divita, G., and Reed, S.I. (2001b). UBA domains of DNA damage-inducible proteins interact with ubiquitin. Nat. Struct. Biol. *8*, 417–422.

Biederer, T., Volkwein, C., and Sommer, T. (1997). Role of Cue1p in ubiquitination and degradation at the ER surface. Science *278*, 1806–1809.

Bilodeau, P.S., Urbanowski, J.L., Winistorfer, S.C., and Piper, R.C. (2002). The Vps27p-Hse1p complex binds ubiquitin and mediates endosomal protein sorting. Nat. Cell Biol. *4*, 534–539.

Bonifacino, J.S., and Traub, L.M. (2003). Signals for sorting of transmembrane proteins to endosomes and lysosomes. Annu. Rev. Biochem., in press.

Buchberger, A. (2002). From UBA to UBX: new words in the ubiquitin vocabulary. Trends Cell Biol. *12*, 216–221.

Brünger, A.T., Adams, P.D., Clore, G.M., DeLano, W.L., Gros, P., Grosse-Kunstleve, R.W., Jiang, J.S., Kuszewski, J., Nilges, M., Pannu, N.S., et al. (1998). Crystallography and NMR system (CNS): a new software system for macromolecular structure determination. Acta Crystallogr. D *54*, 905–921.

Burd, C.G., Mustol, P.A., Schu, P.V., and Emr, S.D. (1996). A yeast protein related to a mammalian ras-binding protein, Vps9p, is required for localization of vacuolar proteins. Mol. Cell. Biol. *16*, 2369–2377.

Burns, K., Clatworthy, J., Martin, L., Martinon, F., Plumpton, C., Maschera, B., Lewis, A., Ray, K., Tschopp, J., and Volpe, F. (2000). Tollip, a new component of the IL-1RI pathway, links IRAK to the IL-1 receptor. Nat. Cell Biol. *2*, 346–351.

CCP4 (Collaborative Computational Project 4) (1994). The CCP4 suite: programs for protein crystallography. Acta Crystallogr. D *50*, 760–763.

Chen, L., Shinde, U., Ortolan, T.G., and Madura, K. (2001). Ubiquitin-associated (UBA) domains in Rad23 bind ubiquitin and promote inhibition of multi-ubiquitin chain assembly. EMBO Rep. *24*, 933–938.

Davies, B.A., Topp, J.D., Sfeir, A.J., Katzmann, D.J., Carney, D.S., Tall, G.G., Friedberg, A.S., Deng, L., Chen, Z., and Horazdovsky, B. (2003). Vps9p CUE domain ubiquitin binding is required for efficient endocytic protein traffic.

Deveraux, Q., Ustrell, V., Pickart, C., and Rechsteiner, M. (1994). A 26 S protease subunit that binds ubiquitin conjugates. J. Biol. Chem. *269*, 7059–7061.

Dieckmann, T., Withers-Ward, E.S., Jarosinksi, M.A., Liu, C.-F., Chen, I.S.Y., and Feigon, J. (1998). Structure of a human DNA repair protein UBA domain that interacts with HIV-1 Vpr. Nat. Struct. Biol. *5*, 1042–1047.

Donaldson, K.M., Yin, H., Gakakis, N., Supek, F., and Joazeiro, C.A. (2003). Ubiquitin signals protein trafficking via interaction with a novel ubiquitin binding domain in the membrane fusion regulator Vps9p. Curr. Biol. *13*, 258–262.

Fang, S., Ferrone, M., Yang, C., Jensen, J.P., Tiwari, S., and Weissman, A.M. (2001). The tumor autocrine motility factor receptor, gp78, is a ubiquitin protein ligase implicated in degradation from the endoplasmic reticulum. Proc. Natl. Acad. Sci. USA *98*, 14422–14427.

Funakoshi, M., Sasaki, T., Nishimoto, T., and Kobayashi, H. (2002). Budding yeast Dsk2p is a polyubiquitin-binding protein that can interact with the proteasome. Proc. Natl. Acad. Sci. USA *99*, 745–750.

Guex, N., and Peitsch, M.C. (1997). SWISS-MODEL and the Swiss-PdbViewer: an environment for comparative protein modeling. Electrophoresis *18*, 2714–2723.

Hama, H., Tall, G.G., and Horazdovsky, B.F. (1999). Vps9p is a guanine nucleotide exchange factor involved in vesicle-mediated vacuolar protein transport. J. Biol. Chem. *274*, 15284–15291.

Hershko, A., and Ciechanover, A. (1998). The ubiquitin system. Annu. Rev. Biochem. *67*, 425–479.

Hicke, L. (2001). A new ticket for entry into budding vesicles-ubiquitin. Cell *106*, 527–530.

Hochstrasser, M. (2000). Evolution and function of ubiquitin-like protein-conjugation systems. Nat. Cell Biol. *2*, E153–E157.

Hofmann, K., and Bucher, P. (1996). The UBA domain: a sequence motif present in multiple enzyme classes of the ubiquitination pathway. Trends Biochem. Sci. *21*, 172–173.

Hofmann, K., and Falquet, L. (2001). A ubiquitin-interacting motif conserved in components of the proteasomal and lysosomal protein degradation systems. Trends Biochem. Sci. *26*, 347–350.

Jenkins, T.M., Engelman, A., Ghirlando, R., and Craigie, R. (1996). A soluble active mutant of HIV-1 integrase: involvement of both the core and carboxyl-terminal domains in multimerization. J. Biol. Chem. *271*, 7712–7718.

Jones, T.A., Zou, J.Y., Cowan, S.W., and Kjelgaard, M. (1991). Improved methods for building protein models in electron density maps and the location of errors in these models. Acta Crystallogr. A *47*, 110–119.

Jullien-Flores, V., Dorseuil, O., Romero, F., Letourneur, F., Saragosti, S., Berger, R., Tavitian, A., Gacon, G., and Camonis, J.H. (1995). Bridging Ral GTPase to Rho pathways. RLIP76, a Ral effector with CDC42/Rac GTPase-activating protein activity. J. Biol. Chem. *270*, 22473–22477.

Katzmann, D.J., Babst, M., and Emr, S.D. (2001). Ubiquitin-dependent sorting into the multivesicular body pathway requires the function of a conserved endosomal protein sorting complex, ESCRT-I. Cell *106*, 145–155.

Klapisz, E., Sorokina, I., Lemeer, S., Pijnenburg, M., Berkleij, A.J., and Henegouwen, P.M. (2002). A ubiquitin-interacting motif (UIM) is essential for Eps15 and Eps15R ubiquitination. J. Biol. Chem. *277*, 30746–30753.

Liu, Y., and Eisenberg, D. (2002). 3D domain swapping: as domains continue to swap. Protein Sci. *11*, 1285–1299.

Longenecker, K.L., Garrard, S.M., Sheffield, P.M., and Derewenda, Z.S. (2001). Protein crystallization by rational mutagenesis of surface residues: Lys to Ala mutations promote crystallization of RhoGDI. Acta Crystallogr. D *57*, 679–688.

Mueller, T.D., and Feigon, J. (2002). Solution structures of the UBA domains reveal a conserved hydrophobic surface for protein-protein interactions. J. Mol. Biol. *319*, 1243–1255.

Oldham, C.E., Mohney, R.P., Miller, S.L.H., Hanes, R.N., and O'Bryan, J.P. (2002). The ubiquitin-interacting motifs target the en-

docytic adaptor protein epsin for ubiquitination. Curr. Biol. *12*, 1112–1116.

Otwinowski, Z., and Minor, W. (1997). Processing of X-ray diffraction data collected in oscillation mode. Methods Enzymol. *276*, 307–326.

Perkins, S.J. (1986). Protein volumes and hydration effects. The calculations of partial specific volumes, neutron scattering matchpoints and 280-nm absorption coefficients for proteins and glycoproteins from amino acid sequences. Eur. J. Biochem. *15*, 169–180.

Pickart, C.M. (2001). Ubiquitin enters the new millennium. Mol. Cell *8*, 499–504.

Polo, S., Sigismund, S., Faretta, M., Guidi, M., Capua, M.R., Bossi, G., Chen, H., De Camilli, P., and Di Fiore, P.P. (2002). A single motif responsible for ubiquitin recognition and monoubiquitination in endocytic proteins. Nature *416*, 451–455.

Ponting, C.P. (2000). Proteins of the endoplasmic-reticulum-associated degradation pathway: domain detection and function prediction. Biochem. J. *351*, 527–535.

Ponting, C.P. (2002). Novel domains and orthologues of eukaryotic transcription elongation factors. Nucleic Acids Res. *30*, 3643–3652.

Pornillos, O., Alam, S.L., Rich, R.L., Myszka, D.G., Davis, D.R., and Sundquist, W.I. (2002). Structure and functional interactions of the Tsg101 UEV domain. EMBO J. *21*, 2397–2406.

Raiborg, C., Bache, K.G., Gillooly, D.J., Madshus, I.H., Stang, E., and Stenmark, H. (2002). Hrs sorts ubiquitinated proteins into clathrin-coated microdomains of early endosomes. Nat. Cell Biol. *4*, 394–398.

Shekhtman, A., and Cowburn, D. (2002). A ubiquitin-interacting motif from Hrs binds to and occludes the ubiquitin surface necessary for polyubiquitination in monoubiquitinated proteins. Biochem. Biophys. Res. Commun. *296*, 1222–1227.

Shih, S.C., Sloper-Mould, K.E., and Hicke, L. (2000). Monoubiquitin carries a novel internalization signal that is appended to activated receptors. EMBO J. *19*, 187–198.

Shih, S.C., Katzmann, D.J., Schnell, J.D., Sutanto, M., Emr, S.D., and Hicke, L. (2002). Epsins and Vps27p/Hrs contain ubiquitin-binding domains that function in receptor endocytosis. Nat. Cell Biol. *4*, 389–393.

Shih, S., Prag, G., Francis, S., Sutanto, M., Hurley, J.H., and Hicke, L. (2003). A ubiquitin-binding motif required for intramolecular monoubiquitination, the CUE domain. EMBO J. *22*, 1273–1281.

Sloper-Mould, K.E., Jemc, J.C., Pickart, C.M., and Hicke, L. (2001). Distinct functional surface regions on ubiquitin. J. Biol. Chem. *276*, 30483–30489.

Terwilliger, T.C. (2000). Maximum-likelihood density modification. Acta Crystallogr. D *56*, 965–972.

Terwilliger, T.C., and Berendzen, J. (1999). Automated MAD and MIR structure solution. Acta Crystallogr. D *55*, 849–861.

Vadlamudi, R.K., Joung, I., Strominger, J.L., and Shin, J. (1996). p62, a phosphotyrosine-independent ligand of the SH2 domain of p56lck, belongs to a new class of ubiquitin-binding proteins. J. Biol. Chem. *271*, 20235–20237.

Vida, T.A., and Emr, S.D. (1995). A new vital stain for visualizing vacuolar membrane dynamics and endocytosis in yeast. J. Cell Biol. *128*, 779–792.

Vijay-Kumar, S., Bugg, C.E., and Cook, W.J. (1987). Structure of ubiquitin refined at 1.8 Å resolution. J. Mol. Biol. *194*, 531–544.

Vojtek, A.B., Hollenberg, S.M., and Cooper, J.A. (1993). Mammalian Ras interacts directly with the serine/threonine kinase Raf. Cell *74*, 205–214.

Wilkinson, C.R., Seeger, M., Hartmann-Petersen, R., Stone, M., Wallace, M., Semple, C., and Gordon, C. (2001). Proteins containing the UBA domain are able to bind to multi-ubiquitin chains. Nat. Cell Biol. *3*, 939–943.

Withers-Ward, E.S., Mueller, T.D., Chen, I.S.Y., and Feigon, J. (2000). Biochemical and structural analysis of the interaction between the UBA(2) domain of the DNA repair protein HHR23A and HIV-1 Vpr. Biochemistry *39*, 14103–14112.

Woudstra, E.C., Gilbert, C., Fellows, J., Jansen, L., Brouwer, J., Erdjument-Bromage, H., Tempst, P., and Svejstrup, J.Q. (2002). A Rad26–Def1 complex coordinates repair and RNA pol II proteolysis in response to DNA damage. Nature *415*, 929–933.

Accession Numbers

The coordinates have been deposited in the PDB under identifiers 1MN3 and 1P3Q.

Supplementary data

Table S1. Equilibrium Concentrations of CUE and Ubiquitin Complexes

[a]Data are based on an initial loading concentration of 0.5 mM CUE and 0.5 mM ubiquitin. Equilibrium concentrations were obtained by fitting the sedimentation equilibrium data to the following mathematical models.

Cooperative model:

$$C_r = C_{o,1}\exp[HM_{b1}(r^2 - r^2_o)] + C_{o,2}\exp[HM_{b2}(r^2 - r^2_o)] + C_{o,1}{}^2\exp[\ln(K_{dim}) + 2HM_{b1}(r^2 - r^2_o)] + C_{o,1}C_{o,2}\exp[\ln(K_0) + H(M_{b1} + M_{b2})(r^2 - r^2_o)] + C_{o,1}{}^2C_{o,2}\exp[\ln(K_{dim}) + 2\ln(K_0) + H(2M_{b1} + M_{b2})(r^2 - r^2_o)] + C_{o,1}{}^2C_{o,2}{}^2\exp[\ln(K_{dim}) + 3\ln(K_0) + H(2M_{b1} + 2M_{b2})(r^2 - r^2_o)] + E \quad [1]$$

Noncooperative model:

$$C_r = C_{o,1}\exp[HM_{b1}(r^2 - r^2_o)] + C_{o,2}\exp[HM_{b2}(r^2 - r^2_o)] + C_{o,1}{}^2\exp[\ln(K_{dim}) + 2HM_{b1}(r^2 - r^2_o)] + C_{o,1}C_{o,2}\exp[\ln(K_0) + H(M_{b1} + M_{b2})(r^2 - r^2_o)] + C_{o,1}{}^2C_{o,2}\exp[\ln(K_{dim}) + \ln(K_0) + H(2M_{b1} + M_{b2})(r^2 - r^2_o)] + C_{o,1}{}^2C_{o,2}{}^2\exp[\ln(K_{dim}) + 2\ln(K_0) + H(2M_{b1} + 2M_{b2})(r^2 - r^2_o)] + E, \quad [2]$$

where $C_{o,1}$ is the concentration of Cue at a reference point r_o, $C_{o,2}$ is the reference concentration of ubiquitin, H represents $\omega^2/2RT$, ω is the angular speed in $rads^{-1}$, R is the gas constant, T is the absolute temperature, E is a small baseline correction, and M_{b1} and M_{b2} represent the buoyant molecular masses of Cue and ubiquitin, respectively. Each data set collected at different rotor speeds were analyzed simultaneously on an absorbance based scale (SigmaPlot 8.02 [SPSS, Inc.]) using experimentally determined values for $\ln(K_{dim})$, to yield the global parameter $\ln(K_0)$. This parameter was used to determine values for K_0, K_1, and K_2. Within the experimental precision of the method, identical values of $\ln(K_0) = 6.8 \pm 0.5$ were obtained. This results in values of 900 M^{-1}, 8.1×10^5 M^{-1}, and 900 M^{-1} for K_0, K_1, and K_2, respectively. Based on the error, limits for K_0 and K_2 are 1500 to 540 M^{-1}, whereas limits for K_1 are 22 to 3.0×10^5 M^{-1}. In the case of the L427D CUE, 1:1 and 2:1 mixtures were studied in TCEP containing buffers. Data were analyzed in terms of a noncooperative model (equation 2) to yield an average $\ln(K_0)$ of 5.9 ± 0.3 (Figure 5E–5G) and values of $K_0 = K_2 = 350$ M^{-1} and $K_1 = 700$ M^{-1}. Limits for K_0 and K_2 are 450 to 270 M^{-1}, whereas limits for K_1 are twice these values.